

MVGT: A Multi-view Graph Transformer Based on Spatial Relations for EEG Emotion Recognition

1st Yanjie Cui

School of Computer Science
Beijing University of Posts and Telecommunications
Beijing, China
yanjiecui@bupt.edu.cn

2nd Xiaohong Liu*

School of Computer Science
Beijing University of Posts and Telecommunications
Beijing, China
xiaohongliu@bupt.edu.cn

3rd Jing Liang

School of Computer Science
Beijing University of Posts and Telecommunications
Beijing, China
liangjing18@bupt.edu.cn

4th Yamin Fu

School of Computer Science
Beijing University of Posts and Telecommunications
Beijing, China
fuyamin@bupt.edu.cn

Abstract—Electroencephalography (EEG), a technique that records electrical activity from the scalp using electrodes, plays a vital role in affective computing. However, fully utilizing the multi-domain characteristics of EEG signals remains a significant challenge. Traditional single-perspective analyses often fail to capture the complex interplay of temporal, frequency, and spatial dimensions in EEG data. To address this, we introduce a multi-view graph transformer (MVGT) based on spatial relations that integrates information across three domains: temporal dynamics from continuous series, frequency features extracted from frequency bands, and inter-channel relationships captured through several spatial encodings. This comprehensive approach allows model to capture the nuanced properties inherent in EEG signals, enhancing its flexibility and representational power. Evaluation on publicly available datasets demonstrates that MVGT surpasses state-of-the-art methods in performance. The results highlight its ability to extract multi-domain information and effectively model inter-channel relationships, showcasing its potential for EEG-based emotion recognition tasks.

Index Terms—EEG, emotion recognition, graph transformer, spatial encoding

I. INTRODUCTION

Affective computing is commonly employed for the analysis of emotional states through Human-Computer Interaction (HCI) systems, which collect multimodal data from subjects, including voice signals, self-reports, body gestures and physiological signals. Among these modalities, physiological signals offer distinct advantages as they are directly derived from the subjects' mental states, making it difficult for them to disguise or conceal their emotions. Scalp electroencephalography (EEG), a physiological signal usually used to analyze the cognitive functions of the human brain, is collected using noninvasive electrodes on the scalp [1]. Nowadays, due to its high temporal resolution, portability, and affordability, this method is widely employed to study brain changes in response to emotional stimuli [2].

EEG signals contain rich emotional information in the temporal, frequency, and spatial domains. How to reasonably and effectively utilize information from each domain is a major challenge. Therefore, recent studies have attempted to combine multi-domain information to capture complex EEG features [3]–[5]. Although these works have achieved good performance, their limited use of domain-specific information has constrained model performance.

The frequency domain features of EEG commonly include power spectral density (PSD), differential entropy (DE), differential asymmetry (DASM), and others. Among these, DE has been proven to be the simplest and most effective in EEG emotion recognition tasks [6]. DE has the ability to distinguish EEG patterns between high-frequency and low-frequency energy [7].

Given the high temporal resolution of EEG signals, many studies use temporal models to extract sequential information. Recurrent neural networks (RNNs) have significantly improved emotion recognition performance by modeling temporal dependencies [8], [9]. However, their serial structure poses challenges for parallelization. Convolutional neural networks (CNNs) have also been applied to extract temporal features, but their performance is restricted by limited receptive fields [3], [10]. To overcome these difficulties, [4] employs the attention mechanism to capture relationships between time points; however, this method may suffer performance degradation due to time-unaligned events at a single moment.

The spatial domain of EEG is equally crucial for understanding emotional states, as emotions often involve distributed neural circuits rather than isolated regions [11]. Asymmetric activity between the left and right hemispheres can reflect changes in valence and arousal [12]. Message-passing-based graph neural network (MPGNN) methods can effectively capture structural relationships between EEG channels [3], [10], [13], [14]. However, using MPGNN may pose potential risks of over-smoothing and over-squashing, which

*Corresponding author

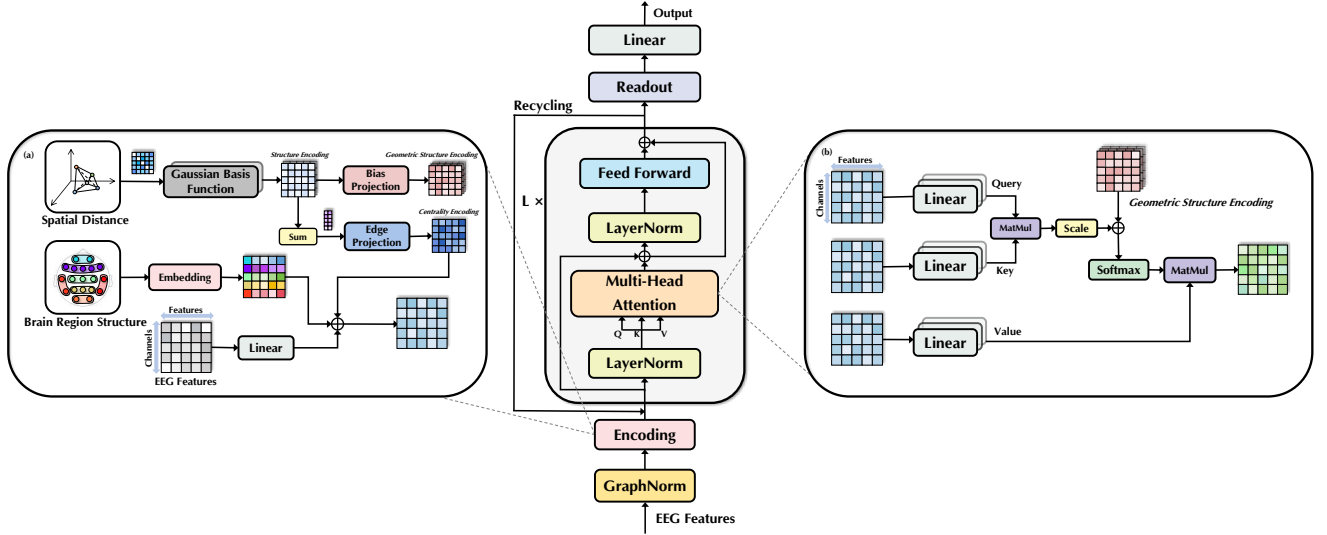


Figure 1. Overall structure of MVGT. (a) represents the process of brain region encoding, centrality encoding and geometric structure encoding. (b) depicts the process of calculating inter-channel correlations based on the attention mechanism and geometric structure encoding. “Recycling” refers to the iterative refinement (see II-D).

could hinder its ability to learn complex representations [15]. Additionally, these methods often underutilize the geometric and anatomical structural relationships inherent in EEG spatial information.

To address these limitations and fully exploit features in the temporal, frequency, and spatial domains, we propose a multi-view graph transformer (MVGT) based on spatial relations for EEG emotion recognition. Graph transformers offer robust and flexible spatial perception while mitigating issues like over-smoothing and over-squashing [15]. For the frequency domain, we use the embedding of DE as the feature representation. For the temporal domain, inspired by [16], we expand the temporal receptive field by embedding entire continuous time segments as tokens and employ feed-forward neural networks to capture temporal patterns. In the spatial domain, we incorporate several simple yet effective spatial encodings, brain region encoding, centrality encoding and geometric structure encoding, into the model to help it capture effective spatial structures. These encodings allow MVGT to adaptively model correlations between EEG channels, delivering improved performance and deeper insights into emotional states.

II. METHODS

A. Problem Definition

EEG signals exhibit an inherent spatial structure that can be represented as a graph $G = (V, E)$, where V denotes the nodes (EEG channels), and E represents the edges (connections between channels). The features of the nodes at time t are denoted by $\mathbf{X}_t = (\mathbf{x}_1, \mathbf{x}_2, \dots, \mathbf{x}_n) \in \mathbb{R}^{n \times f}$, where $n = |V|$ represents the number of nodes and f represents the dimension of DE features extracted on five frequency bands, i.e., δ (1-4Hz), θ (4-8Hz), α (8-14Hz), β (14-31Hz), γ (31-50Hz). To

model the temporal dynamics, continuous segments are extracted using a sliding window. For the s -th segment, the data is represented as $\tilde{\mathbf{X}}_s = (\tilde{\mathbf{x}}_1, \tilde{\mathbf{x}}_2, \dots, \tilde{\mathbf{x}}_n) \in \mathbb{R}^{n \times Tf}$, where T is the window size. The training samples are embedded through an encoding layer, incorporating centrality and brain region encodings to yield $\mathbf{H}_s^0 = (\mathbf{h}_1^0, \mathbf{h}_2^0, \dots, \mathbf{h}_n^0) \in \mathbb{R}^{n \times d}$ (see Fig. 1(a)), where d is the embedding dimension. The encoded data is then input into the model for emotion classification.

B. Temporal Embedding

Temporal information is critical in time-series processing. [4] treated the features of different channels at the same time points as tokens and employed the attention mechanism to extract temporal correlations between them. However, due to anisotropic volume conduction characteristics [17] in human brain tissues, there may be different physical meanings between channels at the same time step, resulting time-unaligned events that subsequently degrade performance. Other approaches [3], [10] utilized CNNs to extract temporal information along the time axis from continuous EEG segments, with the receptive field limited by the size of the convolution kernel. Inspired by [16], we broaden the receptive field by embedding entire time segments as tokens rather than single time points. EEG signals are segmented using overlapping sliding windows of size T , and these segments are treated as tokens. After processing with sliding windows, we obtain $\tilde{\mathbf{X}} = (\tilde{\mathbf{X}}_1, \tilde{\mathbf{X}}_2, \dots, \tilde{\mathbf{X}}_S) \in \mathbb{R}^{S \times n \times Tf}$, where S denotes the number of continuous EEG segments, n is the number of channels, and f denotes the dimension of DE features. Refer to the Appendix B for more temporal embedding details.

According to the universal approximation theorem [18], the feed-forward neural network (FFN), as the basic module of the Transformer [19] encoder, can learn the intrinsic properties to describe a time series. By processing continuous time segments as input, the FFN extracts temporal features independently for each channel, providing more advantageous predictive representations compared to self-attention [16].

C. Spatial Encoding

To better recognize emotional patterns in emotion classification tasks, we employ three effective methods of spatial encoding: brain region encoding (BRE), centrality encoding (CE) and geometric structure encoding (GSE).

1) *Brain Region Encoding*: Neuroscience research indicates that specific brain regions activate together during high-level cognitive processes [20]. In EEG emotion recognition, incorporating relevant neuroscience findings can typically enhance recognition accuracy. For example, studies like [13] and [21] utilized the asymmetry of neural activity between the left and right hemispheres to enhance recognition performance. [10] divided EEG channels into different regions and combined intra-region convolution with inter-region convolution to capture spatial relationships. Building on [10], we propose four learnable BRE schemes based on neuroscience research, ranging from coarse-grained to fine-grained encodings, namely: LOBE, FRONTAL, GENERAL, and HEMISPHERE. The four schemes mentioned above are shown in Fig. 2.

We assign a brain region tag to each electrode, then map the tags into an embedding space using a learnable projection function, and simply add the embeddings to the node features. For node i , the encoding is defined as:

$$\mathbf{r}_i = \text{Embedding}(\text{Tag}(i)), \quad \mathbf{r}_i \in \mathbb{R}^d, \quad (1)$$

where Tag identifies the brain region associated with node i , and nodes within the same brain region share a common embedding vector.

2) *Structure Encoding*: EEG channels are distributed in the 3D space, and the functional connectivity between them remains imprecisely defined. Therefore, inspired by [22], we model the relationships between EEG channels as a fully connected directed graph to avoid making specific assumptions about functional connectivity. Firstly, let $\phi(i, j)$ represent the Euclidean distance between node i and node j , and encode $\phi(i, j)$ using a set of Gaussian basis functions [22], [23]. Let $\mathbf{b}_k \in \mathbb{R}^{n \times n}$ denote one of the Gaussian basis functions. The element (i, j) of this function can be expressed as:

$$\mathbf{b}_k(i, j) = \mathcal{G}_k(\alpha_{ij}\phi(i, j) + \beta_{ij} - \mu_k, \sigma_k), \quad (2)$$

where μ_k (mean), σ_k (variance), α_{ij} , β_{ij} are learnable scalars, and i and j denote the index of the source and target node, respectively. By utilizing multiple Gaussian basis functions, we project the distance ϕ into various distributions. A distance value close to the mean μ_k of the k -th basis function receives higher attention, while the variance σ_k controls the attention's

concentration. This configuration provides flexibility and expressiveness to the encoding. The outputs of these functions are concatenated, forming the structure encoding:

$$\mathbf{B} = \parallel_{k=1}^K \mathbf{b}_k, \quad \mathbf{B} \in \mathbb{R}^{n \times n \times K}, \quad (3)$$

where \parallel denotes the concatenation operator. Secondly, the structure encoding is summed along the second dimension, followed by an edge projection through a linear layer to derive the CE (see (4)) that reflects each node's relative importance. Nodes with higher cumulative weights are considered to have a greater level of involvement within the network. The encoding process for a node in a sample of the input data is as follows:

$$\mathbf{c}_i = \mathbf{e}_i \mathbf{W}_{\mathcal{E}}, \quad \mathbf{e}_{i,k} = \sum_{j=1}^n \mathbf{B}_{i,j,k}, \quad (4)$$

$$\mathbf{h}_i^0 = \tilde{\mathbf{x}}_i \mathbf{W}_{\mathcal{X}} + \mathbf{c}_i + \mathbf{r}_i, \quad (5)$$

$$\mathbf{B}' = \text{Projection}(\mathbf{B}), \quad (6)$$

where i denotes the node index, and k refers to the index of the basis function. The matrix $\mathbf{W}_{\mathcal{X}} \in \mathbb{R}^{Tf \times d}$ represents a linear projection, while $\mathbf{W}_{\mathcal{E}} \in \mathbb{R}^{K \times d}$ is the edge projection. $\text{Projection} : \mathbb{R}^{n \times n \times K} \mapsto \mathbb{R}^{n \times n \times M}$ is a nonlinear transformation for structure encoding to obtain the GSE, where M is the number of attention heads. Finally, We incorporate this encoding as a bias term into the softmax attention (see (8)).

Unlike previous symmetric adjacency matrices [4], [13], our directed spatial encoding matrix allows the model to learn distinct correlations for (i, j) and (j, i) . Letting l denote the model depth, s denote the sample index and m denote the index of multi-head attention, the multi-head attention module (MHA) can be represented as:

$$\mathbf{Q}_s^{l,m} = \mathbf{H}_s^{l-1} \mathbf{W}_{\mathcal{Q}}^{l,m}, \mathbf{K}_s^{l,m} = \mathbf{H}_s^{l-1} \mathbf{W}_{\mathcal{K}}^{l,m}, \mathbf{V}_s^{l,m} = \mathbf{H}_s^{l-1} \mathbf{W}_{\mathcal{V}}^{l,m}, \quad (7)$$

$$\mathbf{Z}_s^{l,m} = \text{Softmax} \left(\frac{\mathbf{Q}_s^{l,m} \mathbf{K}_s^{l,m \top}}{\sqrt{d_h^{l,m}}} + \mathbf{B}'^m \right) \mathbf{V}_s^{l,m}, \quad (8)$$

$$\text{MHA}^l(\mathbf{H}_s^{l-1}) = \left(\parallel_{m=1}^M \mathbf{Z}_s^{l,m} \right) \mathbf{W}_{\mathcal{O}}^l, \quad (9)$$

where the projections $\mathbf{W}_{\mathcal{O}}^l$, $\mathbf{W}_{\mathcal{Q}}^{l,m}$, $\mathbf{W}_{\mathcal{K}}^{l,m}$ and $\mathbf{W}_{\mathcal{V}}^{l,m}$ are learnable model parameters. The scalar $d_h^{l,m}$ is the second dimension of $\mathbf{W}_{\mathcal{K}}^{l,m}$. The GSE bias term \mathbf{B}' is incorporated into the softmax operation, enabling the model to adaptively adjust inter-channel relationships. For example, if $\mathbf{B}'(i, j)$ is a decreasing function, closer nodes will receive higher attention.

The proposed method integrates features from temporal, frequency, and spatial domains, expanding the model's capacity to represent complex EEG signals. By combining GSE with softmax attention, the model captures semantic correlations across nodes from multiple perspectives.

D. Implementation Details of MVGT

In this section, we describe the overall architecture of the model, as illustrated in Fig. 1. For better optimization, we first apply GraphNorm [24] to normalize the input features to a

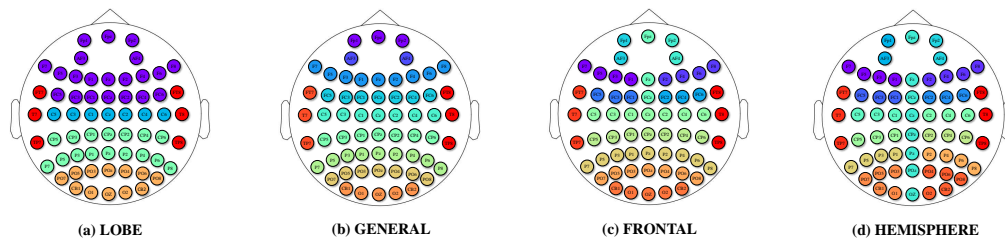


Figure 2. The brain region division schemes are illustrated. (a) LOBE scheme shows a coarse partitioning based on lobe structures. (b) GENERAL scheme represents a fine-grained partitioning of the brain lobes. (c) FRONTAL scheme introduces symmetry of the left and right frontal regions. (d) HEMISPHERE scheme further enhances the channel symmetry in the partitioning scheme. Channels of the same color belong to the same brain region.

range between 0 and 1. The encodings could be characterized as below:

$$\tilde{X}_s^l = \text{GraphNorm}(\tilde{X}_s), \quad (10)$$

$$H_s^0 = \text{Encoding}(\tilde{X}_s^l). \quad (11)$$

We employ a Pre-LN structure, applying layer normalization (LN) before the MHA and the FFN. This design choice is supported by prior research [25], which demonstrates that Pre-LN structures produce more stable gradients, facilitating faster and more reliable convergence. To further prevent overfitting, dropout is employed during training. The process is expressed mathematically as:

$$H_s^l = \text{MHA}^l(\text{LN}(H_s^{l-1})) + H_s^{l-1}, \quad (12)$$

$$H_s^l = \text{FFN}^l(\text{LN}(H_s^l)) + H_s^l. \quad (13)$$

Inspired by [22], [26], we apply iterative refinement by recursively feeding the outputs of the model back into the same modules, denoted as “recycling” in Fig. 1. The iterative approach refines the model’s ability to discriminate encoded information and understand emotional patterns, thereby helping the model capture more effective details.

III. EXPERIMENTS

A. Datasets and Settings

For our experiments, we select the SEED [7] and SEED-IV [27] datasets to evaluate the effectiveness of our model. These datasets consist of EEG signals recorded from subjects watching emotion-eliciting videos. Following the settings of previous studies [3]–[5], [7], [13], [14], [21], [27], we use pre-computed differential entropy (DE) features for the recognition task. Time segments are extracted using an overlapping sliding window of size T , consistent with [3], with T set to 5. For the SEED dataset, we use the first 9 trials of each subject as the training set and the last 6 trials as the test set, as done in previous research. The DE features are computed using five frequency bands extracted from 1s nonoverlapping windows. The model performance is evaluated based on the average accuracy and standard deviation across all subjects over two sessions of EEG data. Similarly, for the SEED-IV dataset, we allocate the first 16 trials to training and the last 8 trials to testing. The DE features for SEED-IV are calculated using 4s windows. The performance of our model is assessed using data

from all three sessions. Refer to Appendix A for DE feature extraction.

Table I

THE CLASSIFICATION ACCURACIES (MEAN/STD) ON SEED AND SEED-IV. MVGT-L, MVGT-G, MVGT-H, MVGT-F: MVGT USING LOBE, GENERAL, HEMISPHERE AND FRONTAL SCHEME. THE BEST RESULTS ARE HIGHLIGHTED IN BOLD, AND THE SECOND-BEST RESULTS ARE UNDERLINED.

Model	SEED	SEED-IV
DGCNN [14]	90.40/08.49	69.88/16.29
BiDANN [9]	92.38/07.04	70.29/12.63
BiHDM [21]	93.12/06.06	74.35/14.09
R2G-STNN [8]	93.34/05.96	-
RGNN [13]	94.24/05.95	79.37/10.54
MD-AGCN [3]	94.81/04.52	87.63/05.77
EmoGT [4]	95.02/05.99	91.20/09.60
MV-SSTMA [5]	95.32/3.05	92.82/5.03
MVGT-L	<u>96.01/04.85</u>	93.20/07.79
MVGT-G	95.82/04.43	94.03/07.77
MVGT-H	95.79/04.90	92.86/08.20
MVGT-F	96.55/04.18	92.92/07.95

During experiments, the hidden dimension is set to 64 and the number of Gaussian basis functions is 32. The number of MHA layers is 4 and the number of attention heads is 2. We employ iterative refinement by recursively feeding the output back into the model for three times. We set the batch size to 32 and the learning rate within the range of $3e-5$ to $3e-3$. Cross-entropy is used as the loss function, and AdamW [28] is employed as the optimizer with a weight decay rate of 0.1.

negative	95.61	3.31	1.08	
neutral	2.71	96.26	1.03	
positive	0.76	1.53	97.70	
	negative	neutral	positive	
neutral	95.77	1.79	0.60	1.84
sad	1.46	93.43	4.38	0.73
fear	1.10	3.38	95.05	0.48
happy	0.96	5.81	2.93	90.30
	neutral	sad	fear	happy
	(a) SEED	(b) SEED-IV		

Figure 3. Confusion matrices of MVGT. (a) Confusion matrix of MVGT-F on SEED. (b) Confusion matrix of MVGT-G on SEED-IV. Each row of the matrix represents the true labels while each column serves as the predicted labels.

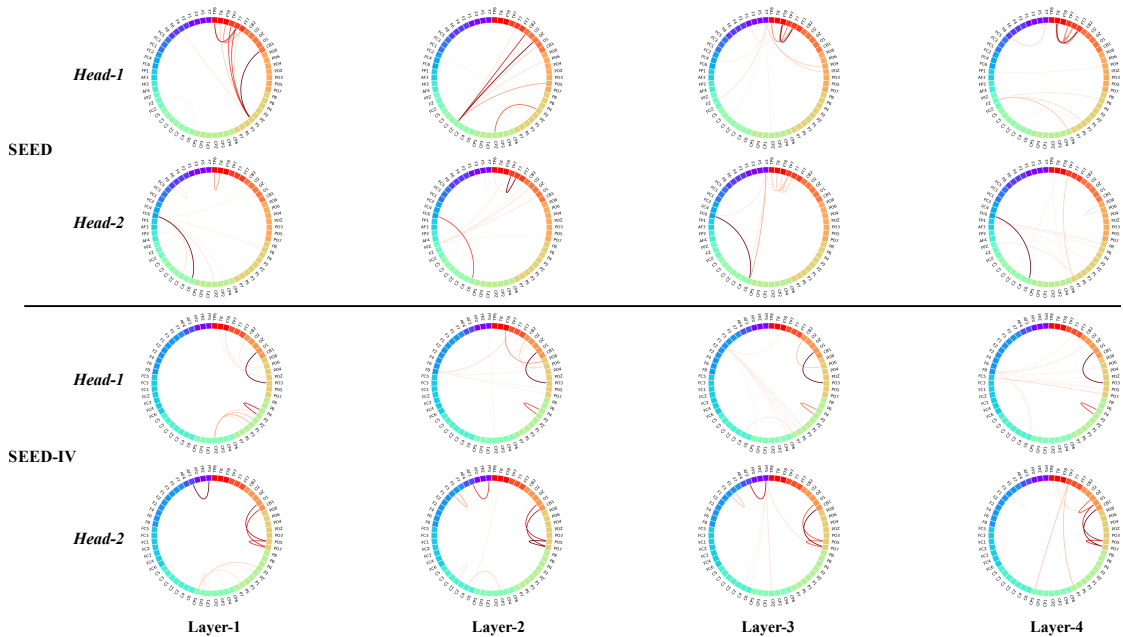


Figure 4. The learned inter-channel relationships from the SEED by the MVGT-F and from the SEED-IV by the MVGT-G are illustrated. The figures show the results of the last iteration in the iterative refinement, highlighting the top 10 channel pairs with the highest weights after softmax (darker colors indicate higher weights). Channels of the same brain region are represented in the same color. Rows correspond to attention heads, while columns represent the layers of the MHA mechanism.

B. Results Analysis

We compare the classification results on the SEED and SEED-IV datasets with recent state-of-the-art models, as shown in Table I. Under identical experimental conditions, our proposed model demonstrated significantly better results than the baselines. On the SEED dataset, the FRONTAL scheme achieved the highest classification accuracy of 96.55%, representing a 1.23% improvement over the best baseline model. Similarly, on the SEED-IV dataset, the GENERAL scheme reached an accuracy of 94.03%, exceeding the best baseline by 1.21%. The differences in accuracy across region division schemes likely result from their data-dependent nature. This suggests that designing data-specific division schemes can enable the model to better utilize data characteristics, thereby enhancing recognition performance. Conversely, improper schemes may result in poor performance.

Fig. 3 shows the confusion matrices for MVGT-F on SEED and MVGT-G on SEED-IV. For SEED, the model achieves 97.70% accuracy for positive emotions but performs less effectively on negative emotions (95.61%). Misclassification rates are low, with 0.76% of positive samples misclassified as negative and 1.08% of negative samples as positive, demonstrating effectiveness in distinguishing valence changes. For SEED-IV, the model achieves its best performance on neutral emotions (95.77%) but slightly lower accuracy on happy emotions (90.30%), likely due to the GENERAL scheme’s sensitivity to balanced emotions.

C. Ablation Study

To validate the effectiveness of our proposed method, we conduct ablation experiments on MVGT-F (based on SEED) and MVGT-G (based on SEED-IV). These experiments incrementally remove four key components: centrality encoding (CE), brain region encoding (BRE), geometric structure encoding (GSE), and the inverted temporal embedding (Inverted). GSE is incorporated into the attention mechanism as a bias (as detailed in (8)). The term “Inverted” refers to embedding continuous time segments as tokens (described in Section II-B), whereas the default approach treats multi-channel information from a single time point as tokens.

Applying the “Inverted” method to the default pure Transformer improves model accuracy by 0.8% on SEED and 0.71% on SEED-IV, highlighting the benefit of encoding continuous temporal information. Among the spatial encoding components, GSE has the greatest impact. Its inclusion in the atten-

Table II
ABLATION STUDY FOR THE CLASSIFICATION ACCURACIES (MEAN/STD) OF MVGT-F ON SEED AND MVGT-G ON SEED-IV. SYMBOL “✓” INDICATES THE COMPONENT IS EMPLOYED.

Centrality	BRE	GSE (bias (8))	Inverted	SEED	SEED-IV
-	-	-	-	92.49/07.58	87.40/11.36
-	-	-	✓	93.29/06.93	88.11/10.30
-	✓	-	✓	94.02/06.30	88.65/10.39
✓	-	-	✓	94.01/05.96	89.25/09.49
✓	✓	-	✓	94.17/05.33	89.58/09.25
-	-	✓	✓	93.79/07.15	89.49/10.40
-	✓	✓	✓	95.10/05.01	91.46/09.75
✓	-	✓	✓	95.05/05.09	92.82/07.95
✓	✓	✓	✓	96.55/04.18	94.03/07.77

tion mechanism increases accuracy by an average of 1.25% on SEED and 3.05% on SEED-IV. In comparison, incorporating BRE improves accuracy by 0.93% (SEED) and 1.01% (SEED-IV), while CE contributes average accuracy gains of 0.90% (SEED) and 1.99% (SEED-IV). These results demonstrate the effectiveness of the temporal embedding method and spatial encoding components in enhancing the model’s ability to classify emotion labels. Moreover, integrating all four components maximizes the model’s overall performance, underscoring their complementary roles in capturing complex EEG patterns.

D. Visualization of Inter-channel Relations

To better illustrate the inter-channel correlations, we visualize the channel relationships captured by MVGT-F on the SEED dataset and MVGT-G on the SEED-IV dataset. From the final MHA layer of the last iterative refinement, we select the top 10 strongest connections. Fig. 4 displays the average weights across all subjects.

On the SEED dataset, the parameters suggest that emotional patterns involve activity across multiple brain regions. The parameters from head-1 in MVGT-F suggest that brain activity is primarily concentrated in the temporal and frontal regions on the lateral side of the brain, which aligns with previous research [4], [7], [13]. Notably, the channel connections (TP8, T7), (FT8, T7), and (T8, FT7) reveal a strong correlation between the left and right hemispheres. The connection (FC6, C6) in head-2 shows the strongest activity, further indicating that local information in the central region may play a key role in emotion recognition.

For the SEED-IV dataset, the strongest inter-channel connections occur in the frontal, parietal, and occipital regions, consistent with existing findings [13]. In MVGT-G, the main channel connections are (O1, PO3), (P4, P2), (CB1, PO7), and (PO5, PO7). Additionally, the connection between AF3 and FP1 provides critical insights into emotion processing, in line with [4], [13].

Our model incorporates both intra-regional and inter-regional brain dynamics, highlighting the critical role of distributed network interactions in modeling emotional states, as discussed by [29].

IV. CONCLUSIONS

This paper presents a multi-view graph transformer (MVGT) based on spatial relations for EEG-based emotion recognition. Our model systematically leverages the frequency, temporal, and spatial properties of EEG data. In the frequency domain, we utilize differential entropy of EEG signals as the basis for emotion recognition. In the temporal domain, we extend the temporal receptive field to capture temporal dynamics from continuous time segments. Additionally, we integrate three spatial encodings into the model to enhance its expressive power and adaptability to spatial structures. Extensive experiments on public emotion recognition datasets demonstrate that our proposed model outperforms other competitive baselines. Furthermore, an analysis of inter-channel correlations indicates that emotional brain activity emerges

from the coordinated interaction of multiple brain regions rather than isolated areas.

REFERENCES

- [1] Soraia M Alarcao and Manuel J Fonseca, “Emotions recognition using eeg signals: A survey,” *IEEE transactions on affective computing*, vol. 10, no. 3, pp. 374–393, 2017.
- [2] Christopher Niemic, “Studies of emotion: a theoretical and empirical review of psychophysiological studies of emotion.,” *Journal of Undergraduate Research*, 2004.
- [3] Rui Li, Yiting Wang, and Bao-Liang Lu, “A multi-domain adaptive graph convolutional network for eeg-based emotion recognition,” in *Proceedings of the 29th ACM International Conference on Multimedia*, 2021, pp. 5565–5573.
- [4] Wei-Bang Jiang, Xu Yan, Wei-Long Zheng, and Bao-Liang Lu, “Elastic graph transformer networks for eeg-based emotion recognition,” in *ICASSP 2023-2023 IEEE International Conference on Acoustics, Speech and Signal Processing (ICASSP)*. IEEE, 2023, pp. 1–5.
- [5] Rui Li, Yiting Wang, Wei-Long Zheng, and Bao-Liang Lu, “A multi-view spectral-spatial-temporal masked autoencoder for decoding emotions with self-supervised learning,” in *Proceedings of the 30th ACM International Conference on Multimedia*, 2022, pp. 6–14.
- [6] Ruo-Nan Duan, Jia-Yi Zhu, and Bao-Liang Lu, “Differential entropy feature for eeg-based emotion classification,” in *2013 6th international IEEE/EMBS conference on neural engineering (NER)*. IEEE, 2013, pp. 81–84.
- [7] Wei-Long Zheng and Bao-Liang Lu, “Investigating critical frequency bands and channels for eeg-based emotion recognition with deep neural networks,” *IEEE Transactions on autonomous mental development*, vol. 7, no. 3, pp. 162–175, 2015.
- [8] Yang Li, Wenming Zheng, Lei Wang, Yuan Zong, and Zhen Cui, “From regional to global brain: A novel hierarchical spatial-temporal neural network model for eeg emotion recognition,” *IEEE Transactions on Affective Computing*, vol. 13, no. 2, pp. 568–578, 2022.
- [9] Yang Li, Wenming Zheng, Yuan Zong, Zhen Cui, Tong Zhang, and Xiaoyan Zhou, “A bi-hemisphere domain adversarial neural network model for eeg emotion recognition,” *IEEE Transactions on Affective Computing*, vol. 12, no. 2, pp. 494–504, 2018.
- [10] Yi Ding, Neethu Robinson, Chengxuan Tong, Qiuhaio Zeng, and Cuntai Guan, “Lgnet: Learning from local-global-graph representations for brain–computer interface,” *IEEE Transactions on Neural Networks and Learning Systems*, pp. 1–14, 2023.
- [11] Iris B Mauss and Michael D Robinson, “Measures of emotion: A reviews,” *Cognition and emotion*, pp. 109–137, 2010.
- [12] Louis A Schmidt and Laurel J Trainor, “Frontal brain electrical activity (eeg) distinguishes valence and intensity of musical emotions,” *Cognition & Emotion*, vol. 15, no. 4, pp. 487–500, 2001.
- [13] Peixiang Zhong, Di Wang, and Chunyan Miao, “Eeg-based emotion recognition using regularized graph neural networks,” *IEEE Transactions on Affective Computing*, vol. 13, no. 3, pp. 1290–1301, 2020.
- [14] Tengfei Song, Wenming Zheng, Peng Song, and Zhen Cui, “Eeg emotion recognition using dynamical graph convolutional neural networks,” *IEEE Transactions on Affective Computing*, vol. 11, no. 3, pp. 532–541, 2018.
- [15] Luis Müller, Mikhail Galkin, Christopher Morris, and Ladislav Rampásek, “Attending to graph transformers,” *Transactions on Machine Learning Research*, 2024.
- [16] Yong Liu, Tengge Hu, Haoran Zhang, Haixu Wu, Shiyu Wang, Lintao Ma, and Mingsheng Long, “itransformer: Inverted transformers are effective for time series forecasting,” in *The Twelfth International Conference on Learning Representations*, 2024.
- [17] Alexander Craik, Yongtian He, and Jose L Contreras-Vidal, “Deep learning for electroencephalogram (eeg) classification tasks: a review,” *Journal of neural engineering*, vol. 16, no. 3, pp. 031001, 2019.
- [18] Kurt Hornik, “Approximation capabilities of multilayer feedforward networks,” *Neural networks*, vol. 4, no. 2, pp. 251–257, 1991.
- [19] Ashish Vaswani, Noam Shazeer, Niki Parmar, Jakob Uszkoreit, Llion Jones, Aidan N Gomez, Łukasz Kaiser, and Illia Polosukhin, “Attention is all you need,” *Advances in neural information processing systems*, vol. 30, 2017.
- [20] Hedy Kober, Lisa Feldman Barrett, Josh Joseph, Eliza Bliss-Moreau, Kristen Lindquist, and Tor D Wager, “Functional grouping and cortical–subcortical interactions in emotion: a meta-analysis of neuroimaging studies,” *Neuroimage*, vol. 42, no. 2, pp. 998–1031, 2008.

- [21] Yang Li, Lei Wang, Wenming Zheng, Yuan Zong, Lei Qi, Zhen Cui, Tong Zhang, and Tengfei Song, "A novel bi-hemispheric discrepancy model for eeg emotion recognition," *IEEE Transactions on Cognitive and Developmental Systems*, vol. 13, no. 2, pp. 354–367, 2020.
- [22] Yu Shi, Shuxin Zheng, Guolin Ke, Yifei Shen, Jiacheng You, Jiyan He, Shengjie Luo, Chang Liu, Di He, and Tie-Yan Liu, "Benchmarking graphormer on large-scale molecular modeling datasets," *arXiv preprint arXiv:2203.04810*, 2022.
- [23] Muhammed Shuaibi, Adeesh Kolluru, Abhishek Das, Aditya Grover, Anuroop Sriram, Zachary Ulissi, and C Lawrence Zitnick, "Rotation invariant graph neural networks using spin convolutions," *arXiv preprint arXiv:2106.09575*, 2021.
- [24] Tianle Cai, Shengjie Luo, Keyulu Xu, Di He, Tie-yan Liu, and Liwei Wang, "Graphnorm: A principled approach to accelerating graph neural network training," in *International Conference on Machine Learning*. PMLR, 2021, pp. 1204–1215.
- [25] Ruibin Xiong, Yunchang Yang, Di He, Kai Zheng, Shuxin Zheng, Huishuai Zhang, Yanyan Lan, Liwei Wang, and Tie-Yan Liu, "On layer normalization in the transformer architecture," 2020.
- [26] John Jumper, Richard Evans, Alexander Pritzel, Tim Green, Michael Figurnov, Olaf Ronneberger, Kathryn Tunyasuvunakool, Russ Bates, Augustin Židek, Anna Potapenko, et al., "Highly accurate protein structure prediction with alphafold," *Nature*, vol. 596, no. 7873, pp. 583–589, 2021.
- [27] Wei-Long Zheng, Wei Liu, Yifei Lu, Bao-Liang Lu, and Andrzej Cichocki, "Emotionmeter: A multimodal framework for recognizing human emotions," *IEEE transactions on cybernetics*, vol. 49, no. 3, pp. 1110–1122, 2018.
- [28] Ilya Loshchilov and Frank Hutter, "Decoupled weight decay regularization," in *International Conference on Learning Representations*, 2019.
- [29] Lisa Feldman Barrett and Ajay Bhaskar Satpute, "Large-scale brain networks in affective and social neuroscience: towards an integrative functional architecture of the brain," *Current opinion in neurobiology*, vol. 23, no. 3, pp. 361–372, 2013.